# Heat capacity of wadeite-type K2Si4O9 and the pressure-induced stable decomposition of K-feldspar

**Article** *in* Contributions to Mineralogy and Petrology · April 1998

DOI: 10.1007/s004100050389



**4 authors**, including:

Bernd Wunder
Helmholtz-Zentrum Potsdam - Deutsches GeoForschungsZentrum GFZ
**424** PUBLICATIONS **3,216** CITATIONS
SEE PROFILE

Günther W. H. Höhne
Ulm University
**147** PUBLICATIONS **3,237** CITATIONS
SEE PROFILE

Contrib Mineral Petrol (1998) 131: 210–218 

**Detlef W. Fasshauer · Bernd Wunder**
**Niranjan D. Chatterjee · Günther W. H. Höhne**

# Heat capacity of wadeite-type $K_2Si_4O_9$ and the pressure-induced stable decomposition of K-feldspar

Received: 11 June 1997 / Accepted: 2 December 1997

**Abstract** The heat capacity of synthetic, stoichiometric wadeite-type $K_2Si_4O_9$ has been measured by DSC in the $195 \leq T(K) \leq 598$ range. Near the upper temperature limit of our data, the heat capacity observed by DSC agrees with that reported by Geisinger et al. (1987) based on a vibrational model of their infrared and Raman spectroscopic data. However, with decreasing temperature, the Cp observed by DSC is progressively higher than that predicted from the vibrational model, suggesting that the standard entropy of $K_2Si_4O_9$ is likely to be larger than $198.9 \pm 4.0$ J/K · mol computed from the spectroscopic data. A fit to the DSC data gave: $Cp(T) = 499.13\ (\pm 1.87) - 4.35014 \cdot 10^3 (\pm 3.489 \cdot 10^1) \cdot T^{-0.5}$, with $T$ in K and average absolute percent deviation of 0.37%. The room-temperature compressibilities of kalsilite and leucite, hitherto unknown, have been measured as well. The data, fitted to the Murnaghan equation of state, gave $K_o = 58.6$ GPa, $K_o' = 0.1$ for kalsilite and $K_o = 45$ GPa, $K_o' = 5.7$ for α-leucite. Apart from the above mentioned data on the properties of the individual phases, we have also obtained reaction-reversals on four equilibria in the system $K_2O$-$Al_2O_3$-$SiO_2$. The Bayesian method has been used simultaneously to process the properties of 13 phases and 15 reactions between them to derive an internally consistent thermodynamic dataset for the $K_2O$-$Al_2O_3$-$SiO_2$ ternary. The enthalpy of formation of $K_2Si_4O_9$ wadeite is in perfect agreement with its revised calorimetric value, the standard entropy is $232.1 \pm 10.4$ J/K · mol, ~15% higher than that implied by vibrational modeling. The phase diagram, generated from our internally consistent thermodynamic dataset, shows that for all probable $P$-$T$ trajectories in the subduction regime, the *stable* pressure-induced decomposition of K-feldspar will produce coesite + kalsilite rather than coesite + kyanite + $K_2Si_4O_9$ (cf. Urakawa et al. 1994).

D.W. Fasshauer · B. Wunder · N.D. Chatterjee (✉)
Institute of Mineralogy, Ruhr University,
D-44780 Bochum, Germany Fax: +49-234-7094 433;
E-mail: Niranjan.Chatterjee@ruhr-uni-bochum.de

G.W.H. Höhne
University of Ulm, Section for Calorimetry, D-89069 Ulm, Germany

B. Wunder
Geoforschungszentrum Potsdam, D-14473 Potsdam, Germany

Editorial responsibility: W. Schreyer

## Introduction

Kinomura et al. (1975) first suggested that, with increasing pressure, K-feldspar decomposes to coesite, kyanite, and the compound $K_2{}^{[VI]}Si[Si_3O_9]$. They also demonstrated that the latter compound is isostructural with the naturally occurring mineral wadeite, $K_2{}^{[VI]}Zr[Si_3O_9]$, the Si in octahedral site substituting for Zr. For the sake of convenience, we shall dub the Si-analogue of wadeite as "Si-wadeite" (SWd for short). Occurrence of Si in both six- and four-fold sites being a novelty at that time, SWd drew the interest of a number of workers. Swanson and Prewitt (1983) solved its crystal structure, while Swanson and Prewitt (1986) and Ross et al. (see Geisinger et al. 1987) reported on its volume equation of state. Geisinger et al. (1987) performed calorimetry and came up with its enthalpy of formation. They also calculated its standard entropy and superambient heat capacity based on vibrational models of infrared and Raman spectroscopic data. These data, along with those from Robie et al. (1978), permitted them to compute the $P$-$T$ curve for the equilibrium coesite (Cs) + kyanite (Ky) + Si-wadeite (SWd) = 2 K-feldspar (Kfs). Their calculated $P$-$T$ curve agreed with the synthesis data of Kinomura et al. (1975) for Kfs on the one hand and the assemblage Cs + Ky + SWd on the other.

More recently, Urakawa et al. (1994) reversed the equilibrium Cs + Ky + SWd = 2 Kfs by in-situ synchrotron radiation study. Their reversed $P$-$T$ curve did *not* agree with that computed by Geisinger et al. (1987); however, they gave no explanation for this disparity. In the meanwhile, a revised value for the enthalpy

of formation of SWd has become available (A. Navrotsky, personal communication 1996). Also available are Robie and Hemingway's (1995) thermodynamic data tables, which are stated to have "entirely superseded" the previous edition (Robie et al. 1978), based on which Geisinger et al. (1987) performed their calculations. While the enthalpy of formation for $K_2O$ remained unchanged, those for a number of K-bearing phases (including K-feldspar) have undergone substantial revision in Robie and Hemingway (1995). If the Urakawa et al. (1994) reversals were to be correct, and likewise the standard entropy and the superambient Cp($T$) computed by Geisinger et al. (1987) from their vibrational model, Bayesian analysis (for details, see Olbricht et al. 1994) shows that the standard enthalpy of formation of SWd must be around −4328 kJ/mol, disagreeing with the revised calorimetric value of −4301.15 ± 5.73 kJ/mol (see Appendix).

The purpose of this paper is to communicate DSC data on the Cp($T$) of SWd, measured in the temperature range 195–598 K, which help resolve the above mentioned discrepancy. Another objective of the present study is to undertake a Bayesian analysis of the system $K_2O$-$Al_2O_3$-$SiO_2$, including most phases of relevance to high-pressure mineral equilibria. The phases to be examined are: α-quartz (aQz), β-quartz (bQz), coesite (Cs), stishovite (Stv), andalusite (And), sillimanite (Si), kyanite (Ky), corundum (Co), kalsilite (Kls), α-leucite (aLc), β-leucite (bLc), K-feldspar (Kfs), and Si-wadeite (SWd). For these phases, most information required for a Bayesian study are already available. By contrast, insufficient thermodynamic data are available for KAlSi$_3O_8$-hollandite; we had to omit it for now from our list. In addition, we have sought to fill up a few gaps by giving new data on the compressibility of kalsilite and leucite. Some phase equilibria reversals have also been made to supplement the existing database and to verify the calculated phase relations. Finally, an internally consistent thermodynamic dataset has been derived, which allows computation of phase equilibria in the $K_2O$-$Al_2O_3$-$SiO_2$ system. In particular, we shall focus on the stable, pressure-induced decomposition of leucite and K-feldspar. It will be shown that for all reasonable $P$-$T$ gradients within the subduction zone, the stable decomposition of K-feldspar leads to the assemblage coesite + kalsilite. By contrast, the stable decomposition of K-feldspar to Si-wadeite + kyanite + coesite is restricted to somewhat lower temperatures, which are of little consequence for the depths of the earth.

## Experimental methods

The experimental techniques required for this work are familiar to most readers; therefore, they will only very briefly be documented.

To synthesize starting materials for determining phase properties (such as compressibility of kalsilite and leucite and molar heat capacity of Si-wadeite) and for reversing several equilibria indicated later, standard cold-seal pressure vessels and an end-loaded piston-cylinder apparatus fitted with "zero friction" NaCl-graphite assemblies of 1.28 and 0.8 cm diameter were used. For the cold-seal apparatus, the uncertainties of $P$ and $T$, due to calibration, gradient and control, are ±5% of $P$ and ±10 °C. The solid-media apparatus with the 1.28 cm assembly has been most recently calibrated (by T. Fockenberg, personal communication) both at ambient and at elevated temperatures. The room-temperature calibration depended on the Bi I–II transition; at higher temperatures, the calibrations relied on farringtonite to $Mg_3(PO_4)_2$-II (Brunet and Vielzeuf 1996) and α-quartz to coesite transitions. At pressures above 5.5 GPa, the 0.8 cm diameter solid-media cell had to be used. B. Wunder has calibrated this assembly at 1050 °C against the $CaGeO_3$ garnet to perovskite transition (Susaki et al. 1985). In no case could a perceptible friction loss be detected. The cumulative uncertainty for $P$ and $T$ in the 5–6.5 GPa and 700–1000 °C range has been estimated as ±0.2 GPa and ±15 °C. For the solid-media runs conducted in the $T$-$P$-range between 900–1050 °C and 1.3–1.6 GPa, the uncertainties are believed to be ±10 °C and ±0.05 GPa.

Gels and glass starting materials, prepared from pure chemicals, were used for synthesizing the phases of interest. While the gels were prepared from $Si(OC_2H_5)_4$, Al powder, and $KHCO_3$ by the technique of Hamilton and Henderson (1968), preparation of the $K_2O \cdot 4SiO_2$ glass for the synthesis of Si-wadeite followed a slightly modified method originally described by Goranson and Kracek (1932). The starting material, a homogenized mixture of $KHCO_3$ and $SiO_2$ of 2:4 molar ratio with 0.24 wt% of excess K, was first slowly heated to 800 °C. After about 24 h, the temperature was slowly raised to 1100 °C. After another 24 h, the melt was quenched to an optically homogeneous glass. Table 1, reproduced later, gives an overview of the starting materials and the synthesis conditions for the individual phases. In all cases, single-phase materials could be prepared. They have been characterized by X-rays, and in one case (SWd) by electron-probe microanalysis (EPMA) as well as $^{29}$Si MAS-NMR spectrometry. The X-ray diffraction data for the determination of the lattice parameters were collected using Si (NBS standard reference material 640) as an internal standard. Least squares refinement of the data was done using the computer program by Appleman and Evans (1973); indexing the diffraction lines was invariably guided by calculated intensities. Table 2 lists the lattice parameters. The EPMA was executed on a Cameca SX 50 device. The working conditions were: accelerating voltage 15 kV, beam current 10 nA, beam diameter 8 μm, counting time 10 s for peak and background. To guard against loss of K, the beam was slowly swivelled around the point to be analyzed. The standard used was a synthetic K-, Mg-, Ca-, and Al-bearing silicate glass. The $^{29}$Si MAS-NMR spectrum of SWd was obtained on a Bruker NMR-spectrometer operated at a resonance frequency of 79.5 MHz, assuming a rather high relaxation time of 300 s for the Si nucleus. The $^{29}$Si MAS-NMR spectrum will be reported relative to the TMS standard.

**Table 1** Details of synthesis of various phases

| Phase | Starting material | $P$ (GPa) | $T$ (°C) | Run duration (days) |
|---|---|---|---|---|
| K-feldspar | Gel | 0.2 | 700 | 2 |
| Kalsilite | Gel | 0.05 | 800 | 7 |
| Leucite | Gel | 0.05 | 800 | 4 |
| Coesite | Glass | 3.5 | 1000 | 1 |
| Kyanite | Gel | 4.5 | 700 | 1 |
| "Si-wadeite" | Glass | 2.5 | 700 | 2 |

**Table 2** Lattice parameters of some of the synthetic phases. The *quantities in parentheses* represent one standard deviation; they apply to the *last* digit(s) of the preceding number

| Phase | Space group | a (Å) | b (Å) | c (Å) | β (°) | V (Å$^3$) |
|---|---|---|---|---|---|---|
| K-feldspar | C2/m | 8.6013(12) | 13.0279(17) | 7.1814(10) | 116.01(1) | 723.23(12) |
| Kalsilite | $P6_3$ | 5.1627(3) | | 8.7115(6) | | 201.08(2) |
| Leucite | $I4_1/a$ | 13.0556(6) | | 13.7560(11) | | 2344.66(23) |
| "Si-wadeite" | $P6_3/m$ | 6.6126(9) | | 9.5101(6) | | 360.13(3) |

Compressibility data for kalsilite and leucite were obtained by in-situ experiments to about 6.1 GPa using the synchrotron radiation facility at HASYLAB, Hamburg. The MAX-80 device, interfaced with a synchrotron source, uses NaCl as an internal pressure calibrant, the equation of state of NaCl (Decker 1966) serves to compute the pressure at each experimental point. On the whole, the standard deviation of $P$ is judged to be about $\pm 0.2$ GPa in that pressure range. The initial compression of the sample at room temperature gave diffraction patterns with broad lines and poor resolution due to the development of deviatoric stress in the pressure medium. Fortunately, stress release was achieved by a short heating of the sample at high pressures to near 500 °C. On subsequent decompression, the pressure medium behaved in a quasihydrostatic fashion. The $P$-$V$ data collected under near-hydrostatic condition were fitted to the Murnaghan equation of state. Table 3 reproduces these data.

The Cp($T$) data for Si-wadeite was obtained by D.W. Fasshauer under the supervision of G.W.H. Höhne at the Calorimetry laboratory of the University of Ulm. Two Perkin-Elmer scanning calorimeters, DSC-2 and DSC-7, were used to measure the Cp($T$) in the temperature ranges 195–330 K and 313–598 K, respectively. Their temperature and heat-flow rate calibrations were accomplished following the recommendations of Höhne et al. (1990) and Sarge et al. (1994). Synthetic SWd, predried at 120 °C, was weighed into Al pans fitted with crimped lids. Sample sizes were 18–25 mg. The determination of the base line made use of identical pan-lid combinations differing less than 0.005 mg from those with the samples. A sapphire single crystal, weighing 129.642 mg, served as reference. The Cp of sapphire was taken from Sarge et al. (1994); it is known to 0.4–0.1% and 0.1–0.2% in the ranges 70–300 K and 290–2250 K, respectively. The heating rate for the measurements, alternately executed on the sample and the standard, was 10 K/min. The measurements were carried out in the interval-scanning mode. Table 4 lists the molar Cp data.

**Table 3** Experimental data on room-temperature compressibility of kalsilite and leucite

| Kalsilite | | Leucite | |
|---|---|---|---|
| Pressure [GPa] | Cell volume [Å$^3$] | Pressure [GPa] | Cell volume [Å$^3$] |
| 0.0001 | 201.08 | 0.0001 | 2344.66 |
| 1.2230 | 197.10 | 1.1150 | 2308.84 |
| 2.1300 | 194.28 | 2.0210 | 2246.61 |
| 1.6060 | 195.66 | 1.0820 | 2290.17 |
| 2.4490 | 193.09 | 1.7440 | 2257.14 |
| 3.5910 | 189.26 | 1.3920 | 2277.03 |
| 4.6690 | 185.05 | 2.3210 | 2228.44 |
| 4.2510 | 187.91 | 1.7960 | 2264.20 |
| 5.2680 | 182.40 | 2.5140 | 2248.79 |
| 6.1400 | 179.86 | 3.5910 | 2188.09 |
| | | 3.5910 | 2199.05 |
| | | 4.6760 | 2150.48 |
| | | 5.7460 | 2132.67 |
| | | 5.1000 | 2155.75 |
| $K_o$ [GPa] = 58.6 | | $K_o$ [GPa] = 45.0 | |
| $K_o' = 0.1$ | | $K_o' = 5.7$ | |

## Experimental results

### Characterization of the synthetic phases

The phases of interest to this study were synthesized from appropriate starting materials under various $P$-$T$ conditions. Table 1 summarizes the synthesis data. Optical and X-ray diffraction studies showed that each synthesis yielded single-phase material.

Table 2 documents the lattice constants of some of the synthetic phases. They are in excellent agreement with literature values. Following Kroll and Ribbe (1983, Eq. 10a, p. 77), the lattice constants of the K-feldspar (sanidine) translate to an Al-occupancy of each T1 site of 0.2942. That corresponds to the non-convergent ordering parameter $Q_t$ (as defined by Carpenter and Salje, 1994) of 0.177. Based on the $T$-dependence of $Q_t$ (see Fig. 5 in Carpenter and Salje, 1994), our synthetic Kfs was slightly more disordered than what would be expected in the event of internal equilibrium. Besides X-rays, our synthetic Si-wadeite was characterized by EPMA and $^{29}$Si MAS-NMR spectrometry. The average of 12 EPMA on SWd grains of 20–50 μm diameter gave $K_{1.991(\pm 0.012)}Si_{4.003(\pm 0.003)}O_9$, indicating that our synthetic Si-wadeite was of stoichiometric composition. Its NMR spectrum comprised two sharp peaks at −95.0 (for $^{[IV]}$Si) and −203.1 ppm (for $^{[VI]}$Si); they had the same intensity ratios as reported by Stebbins and Kanzaki (1991).

### Room-temperature compressibilities of kalsilite and leucite

Table 3 lists the pressure versus cell volume data obtained for kalsilite and leucite, respectively, at ambient temperature in a quasi-hydrostatic medium using a MAX-80 device interfaced to a synchrotron source. The data have been smoothed by Murnaghan equation of state. The bulk modulus $K_o$ and its pressure-derivative, $K_o'$ are indicated at the bottom of the table. As far as we are aware, no previous data on these quantities exist in the literature.

### Molar heat capacity of Si-wadeite

The heat capacity of synthetic Si-wadeite could sucessfully be measured in the temperature range 195–598 K. Viewed under the microscope, the Si-wadeite sample

**Table 4** DSC data on the molar heat capacity for Si-wadeite (SWd)

| $T$ (K) | Cp (J/mol · K) | Wt | $T$ (K) | Cp (J/mol · K) | Wt | $T$ (K) | Cp (J/mol · K) | Wt | $T$ (K) | Cp (J/mol · K) | Wt |
|---|---|---|---|---|---|---|---|---|---|---|---|
| 195.00 | 186.83 | 1.0 | 305.00 | 250.63 | 1.0 | 393.08 | 284.35 | 0.0 | 488.22 | 309.65 | 0.0 |
| 200.00 | 190.23 | 1.0 | 310.00 | 253.50 | 1.0 | 378.23 | 277.21 | 0.5 | 498.22 | 310.15 | 0.0 |
| 205.00 | 194.71 | 1.0 | 315.00 | 255.59 | 0.5 | 388.23 | 281.10 | 1.0 | 508.22 | 310.27 | 0.0 |
| 210.00 | 197.63 | 1.0 | 320.00 | 258.15 | 0.5 | 398.23 | 282.03 | 1.0 | 513.22 | 310.47 | 1.0 |
| 215.00 | 202.26 | 1.0 | 325.00 | 258.50 | 0.5 | 403.23 | 282.92 | 1.0 | 518.22 | 310.34 | 1.0 |
| 220.00 | 204.36 | 1.0 | 330.00 | 261.13 | 0.5 | 408.23 | 284.01 | 1.0 | 523.22 | 310.52 | 1.0 |
| 225.00 | 208.86 | 1.0 | 313.28 | 250.11 | 0.0 | 413.23 | 285.05 | 1.0 | 528.22 | 310.61 | 1.0 |
| 230.00 | 211.56 | 1.0 | 318.22 | 253.02 | 0.5 | 418.23 | 285.97 | 1.0 | 533.22 | 310.37 | 1.0 |
| 235.00 | 215.32 | 1.0 | 323.28 | 255.47 | 0.5 | 423.23 | 286.53 | 1.0 | 538.22 | 310.27 | 1.0 |
| 240.00 | 218.23 | 1.0 | 328.22 | 257.79 | 0.5 | 428.23 | 287.89 | 1.0 | 543.22 | 310.61 | 1.0 |
| 245.00 | 222.01 | 1.0 | 333.28 | 259.71 | 0.5 | 433.22 | 289.84 | 1.0 | 548.22 | 311.17 | 1.0 |
| 250.00 | 224.69 | 1.0 | 338.21 | 261.83 | 1.0 | 438.22 | 290.78 | 1.0 | 553.22 | 312.07 | 1.0 |
| 255.00 | 226.60 | 1.0 | 343.28 | 263.94 | 1.0 | 443.22 | 291.53 | 1.0 | 558.22 | 313.36 | 1.0 |
| 260.00 | 230.46 | 1.0 | 348.21 | 265.85 | 1.0 | 448.22 | 292.24 | 1.0 | 563.22 | 314.91 | 1.0 |
| 265.00 | 231.92 | 1.0 | 353.28 | 267.98 | 1.0 | 453.22 | 292.82 | 1.0 | 568.22 | 316.83 | 1.0 |
| 270.00 | 234.52 | 1.0 | 358.21 | 269.96 | 1.0 | 458.22 | 293.86 | 1.0 | 573.21 | 319.68 | 1.0 |
| 275.00 | 236.61 | 1.0 | 363.28 | 271.68 | 1.0 | 463.22 | 294.91 | 1.0 | 578.21 | 322.81 | 0.0 |
| 280.00 | 240.43 | 1.0 | 368.21 | 273.79 | 1.0 | 468.22 | 296.09 | 1.0 | 588.21 | 331.08 | 1.0 |
| 285.00 | 241.80 | 1.0 | 373.28 | 275.69 | 1.0 | 473.22 | 297.99 | 1.0 | 578.24 | 317.63 | 1.0 |
| 290.00 | 244.05 | 1.0 | 378.21 | 277.76 | 0.5 | 478.22 | 300.06 | 1.0 | 583.24 | 318.76 | 1.0 |
| 295.00 | 246.94 | 1.0 | 383.28 | 279.88 | 0.5 | 488.22 | 304.91 | 1.0 | 588.24 | 320.71 | 1.0 |
| 300.00 | 248.56 | 1.0 | 388.21 | 282.11 | 0.0 | 478.22 | 309.23 | 0.0 | 593.24 | 322.77 | 1.0 |
| | | | | | | | | | 598.24 | 325.26 | 0.0 |

shows xenomorphic to hypidiomorphic crystals having an average grain size of $10 \times 20$ μm, ranging up to $20 \times 60$ μm. Table 4 lists the $T$ versus Cp data. While data scatter was barely a problem, "offsets" of data (very similar to that documented by Komada et al. 1995, Figs. 2 and 7) at the beginning and at the end of each scanning interval increased with rising temperature. Above 593 K, data "offset" and scatter became too strong to permit reliable Cp measurement. The X-ray diffractogram of Si-wadeite exposed to a $T$ slightly above 600 K did not reveal any damage to the sample, nor could any change be observed on an SEM image; thus no obvious explanation for the "offsets" seems to exist. The overall uncertainty of the data is believed to be 1%. Smoothing these data by a least squares fit made use of all datapoints with a percent deviation less than about 1%, eliminating very few "offsets". All datapoints were assigned unit weight, excepting those in the regions of overlap of the scanning intervals, which were weighted 0.5. The Cp($T$) function recommended by Berman and Brown (1985) was used. Of the four fit parameters, only two were adequate to represent the data: $\mathrm{Cp}(T) = 499.13 \quad (\pm 1.87) - 4.35014 \cdot 10^3 \; (\pm 3.489 \cdot 10^1) \cdot T^{-0.5}$, with $T$ given in (K). The average absolute percent deviation of the fit is 0.37%.

It is interesting to compare the DSC data for Cp($T$) of SWd with that computed from a vibrational model of infrared and Raman spectra by Geisinger et al. (1987). Near the upper temperature limit of the DSC measurement, they are essentially identical. However, at lower temperatures, the DSC data are progessively higher. Figure 1 depicts the two sets of data; it is clear that the lower the temperature, the greater the difference between the two. Thus, it seems likely that the standard entropy of SWd will be higher than that given by Geisinger et al. (1987).

## Experimental reversal of some equilibria

A few reversals for the equilibria Kls + Kfs = aLc, Kls + Kfs = bLc, SWd + Ky + Cs = Kfs have been

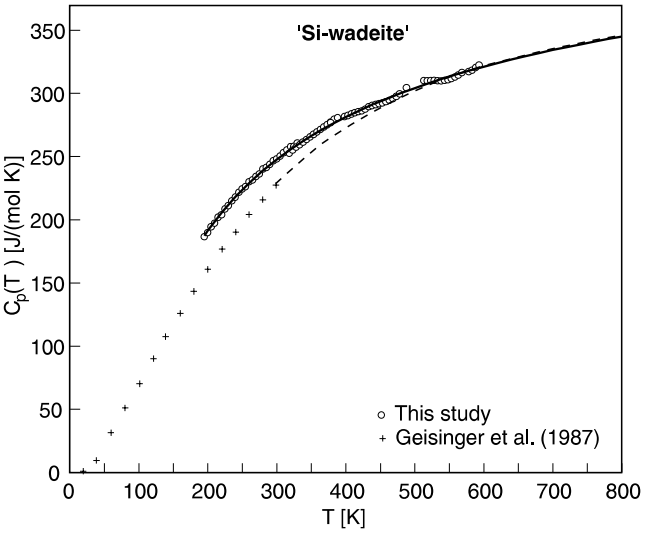


**Fig. 1** Comparison of the heat capacity of "Si-wadeite" obtained by DSC (*circles*) with those calculated from a vibrational model of infrared and Raman spectroscopic data by Geisinger et al. (1987). In the "low-temperature" range the Cp data by Geisinger et al. are shown as *crosses*, their superambient Cp($T$) function by the *dashed line*. The two parameter Cp($T$) fit to our DSC data is represented by the *solid line*

achieved by us to supplement the existing database. A preliminary Bayesian analysis of all phase property and phase equilibria data of the system $K_2O$-$Al_2O_3$-$SiO_2$ gave a set of internally consistent thermodynamic data for the 13 phases of relevance to this study. The *P-T* diagram computed from this "preliminary" set of internally consistent thermodynamic data suggested that SWd + Ky + Cs = Kfs will become metastable above 500 °C; at higher temperatures, the stable equilibrium will be Kls + Cs = Kfs. That has been confirmed by reversing the Kls + Cs = Kfs equilibrium. Tables 5a through 5d document the critical reversal runs. Attention is drawn to the slight but definite change in the order parameter, $Q_t$, of the Kfs during the runs; they indicate a tendency toward achievement of internal equilibrium in the Kfs in course of the runs.

In a subsequent cycle, the complete set of phase property and phase equilibria restrictions from the literature, along with those obtained by us, was processed by the Bayesian method; that led to the "final" internally consistent thermodynamic dataset for the 13 phases of the $K_2O$-$Al_2O_3$-$SiO_2$ system, presented later on in Table 8.

## The refined thermodynamic dataset for the phases of the $K_2O$-$Al_2O_3$-$SiO_2$ system

### The Bayesian approach

To handle simultaneously the phase properties (like standard enthalpies of formation, standard entropies etc.) and phase equilibria restrictions, the Bayesian approach, described in detail by Olbricht et al. (1994), has been adopted. The quality of results obtained by the Bayes method has been illustrated earlier on several occasions (e.g., Chatterjee et al. 1994; Waterwiese et al. 1995; Fasshauer et al. 1997). Only a very brief account of the method needs to be given here. In the Bayesian method, the phase properties (like standard molar enthalpy of formation, $H^\circ_{f,T^\circ}$, molar entropy, $S^\circ_{T^\circ}$, molar heat capacity, $C_p(T)$, standard molar volume, $V^\circ_{T^\circ}$, the temperature-dependence of molar volume $V^\circ(T)$, bulk modulus and its pressure-derivative, $K_o$ and $K_o'$) of each phase is combined with the reaction properties ($\Delta\mu > 0$ for stable reactants and $\Delta\mu < 0$ for stable products) of all reactions between the phases to derive a set of "refined" thermodynamic data, together with their uncertainties and correlations. The term $\Delta\mu$ follows from the relation

$$\Delta\mu = \sum_i \nu_i \mu_i \tag{1}$$

where $\nu_i$ and $\mu_i$ stand for the stoichiometric coefficient and chemical potential of the *i*-th phase component, respectively, the products counting positive and the reactants negative. Because we are concerned with end-member phases in the present context, we may write the chemical potential of the *i*-th substance, $\mu_i$, as

$$\mu_i = H^\circ_{f,T^\circ,i} - T \cdot S^\circ_{T^\circ,i} + \int_{T^\circ}^{T} C_{p,i}(T)\mathrm{d}T - T \cdot \int_{T^\circ}^{T} (C_{p,i}(T)/T)\mathrm{d}T + \int_{P^\circ}^{P} V_i(T,P)\mathrm{d}P + G_{\mathrm{tr},i} \tag{2}$$

**Table 5a** Run data on the reversal of the equilibrium 1 Kls + 1 Kfs = 2 aLc

| *T*(°C) | *P*(GPa) | Run time(h) | Run products | $Q_t$ (starting Kfs) | $Q_t$ (product Kfs) |
|---|---|---|---|---|---|
| 520 | 0.20 | 2975 | Kfs + Kls increase | 0.177 | 0.216 |
| 605 | 0.40 | 913 | Kfs + Kls increase | 0.177 | 0.212 |
| 625 | 0.40 | 861 | Lc increases | 0.177 | – |

**Table 5b** Run data on the reversal of the equilibrium 1 Kls + 1 Kfs = 2 bLc

| *T*(°C) | *P*(GPa) | Run time(h) | Run products | $Q_t$ (starting Kfs) | $Q_t$ (product Kfs) |
|---|---|---|---|---|---|
| 899 | 1.50 | 113 | Kfs + Kls increase | 0.177 | 0.168 |
| 928 | 1.31 | 137 | Lc increases | 0.177 | – |
| 1058 | 1.60 | 44 | Lc increases | 0.177 | – |

**Table 5c** Run data on the reversal of the equilibrium 1 SWd + 1 Ky + 1 Cs = 2 Kfs

| *T*(°C) | *P*(GPa) | Run time(h) | Run products | $Q_t$ (starting Kfs) | $Q_t$ (product Kfs) |
|---|---|---|---|---|---|
| 800 | 6.30 | 96 | Kfs decreases | 0.177 | – |
| 800 | 6.10 | 96 | No reaction | 0.177 | – |
| 800 | 5.90 | 96 | Kfs increases | 0.177 | Not determined |

**Table 5d** Run data on the reversal of the equilibrium 1 Kls + 2 Cs = 1 Kfs

| *T*(°C) | *P*(GPa) | Run time(h) | Run products | $Q_t$ (starting Kfs) | $Q_t$ (product Kfs) |
|---|---|---|---|---|---|
| 700 | 5.30 | 96 | No reaction | 0.177 | – |
| 700 | 5.50 | 168 | Kls + Cs increase | 0.177 | – |
| 1000 | 5.50 | 24 | Kfs increases | 0.177 | 0.237 |

with $V_i(T,P)$, indicating the $T$-$P$-dependence of the molar volume of $i$ and $G_{\mathrm{tr},i}$, the molar Gibbs energy of phase transition of $i$, if there is one in the range $T^\circ$ to $T$ and $P^\circ$ to $P$. The reference temperature and pressure, $T^\circ$ and $P^\circ$, are defined as 298.15 K and 1 bar, respectively. The $T$-dependence of the molar volume, $V^\circ(T)$, will be expressed as

$$V^\circ(T) = V^\circ_{T^\circ} \cdot (1 + v_1 \cdot (T - T^\circ) + v_2 \cdot (T - T^\circ)^2) \quad (3)$$

The $P$-dependence of the molar volume will be treated in terms of the Murnaghan equation. As such, $V(T,P)$ of Eq. (2) at any set of $T$ and $P$ will be given by the expression

$$V(T,P) = V^\circ(T) \cdot \left(1 + \frac{K'_\circ}{K_\circ} \cdot P\right)^{-\frac{1}{K'_\circ}} \quad (4)$$

$K_\mathrm{o}$ and $K_\mathrm{o}'$ being the room-temperature bulk modulus and its pressure-derivative, respectively. Of the various phase properties, only $H^\circ_{f,T^\circ}$, and $S^\circ_{T^\circ}$ will be regarded as variables; therefore, only they need to be refined (i.e. updated subject to the reaction property restrictions, $\Delta\mu > 0$ or $\Delta\mu < 0$), all other quantities will be handled as $T$,$P$-dependent "constants". In other words, the refined set of thermodynamic data will comprise $H^\circ_{f,T^\circ}$ and $S^\circ_{T^\circ}$ for each phase, as well as their uncertainties and correlations. It may be pointed out that the Bayesian technique has to deal with the same two quantities also handled by mathematical programming; however only the former returns the uncertainties for $H^\circ_{f,T^\circ}$ and $S^\circ_{T^\circ}$ and the correlations between them. For an extensive treatment of the relative merits of the two methods, the reader is referred to Olbricht et al. (1994).

## Phase property data

Table 6 summarizes the sources of the phase property data used as input in our Bayesian analysis. $H^\circ_{f,T^\circ}$ and $S^\circ_{T^\circ}$ of most phases are known; in a few cases they had to be estimated. In the Bayes method, the former categories of $H^\circ_{f,T^\circ}$ and $S^\circ_{T^\circ}$ are handled as normally distributed

**Table 6** Sources of the phase property data used as input in Bayes analysis. The reference phases are marked with *asterisks*. Estimated quantities are indicated by the symbol ⊗

| Phase | $H^\circ_{f,T^\circ}$ | $S^\circ_{T^\circ}$ | $C_\mathrm{p}(T)$ | $V^\circ_{T^\circ}$ | $V^\circ(T)$ | $K_\mathrm{o}$, $K_\mathrm{o}'$ |
|---|---|---|---|---|---|---|
| Andalusite | [1] | [1] | [1] | [2] | [3] | [4] |
| Corundum* | [5] | [5] | [1] | [1] | [3] | [6] |
| Coesite | [7] | [7] | [7] | [3] | [3] | [8] |
| K-Feldspar* | [1] | [1] | [9] | [10] | [3] | [11] |
| Kalsilite | ⊗ [1] | [1] | [9], [12] | [1] | [13] | [14] |
| Kyanite | [1] | [1] | [1] | [2] | [3] | [15] |
| "Si-wadeite" | [16] | ⊗ [14] | [14] | [17] | [18] | [18] |
| Sillimanite | [1] | [1] | [1] | [2] | [19] | [3] |
| Stishovite | [7] | [7] | [7] | [20], [21] | [20], [21] | [8] |
| α-Leucite | ⊗ [1] | [1] | [22], [23], [24] | [25] | [25] | [14] |
| α-Quartz* | [5] | [5] | [9], [3] | [1] | [3] | [8] |
| β-Leucite | ⊗ [14] | ⊗ [14] | [22], [23], [24] | [25] | [25] | ⊗ [14] |
| β-Quartz | ⊗ [26] | ⊗ [27] | [9] | [3] | [3] | [3] |

[1] Robie, Hemingway (1995); [2] Holdaway, Mukhopadhyay (1993); [3] Berman (1988); [4] Ralph et al. (1984); [5] Cox et al. (1989); [6] Richet et al. (1988); [7] Akaogi et al. (1995); [8] Hemley et al. (1994); [9] Berman, Brown (1985); [10] Kroll et al. (1986); [11] Angel (1994); [12] Berman, Brown (1986); [13] Henderson, Taylor (1988); [14] This study; [15] Comodi et al. (1997); [16] A. Navrotsky (personal communication); [17] Swanson, Prewitt (1983); [18] Geisinger et al. (1987); [19] Hemingway et al. (1991); [20] Ito et al. (1974); [21] Endo et al. (1986); [22] Kelley et al. (1953); [23] Pankratz (1968); [24] Lange et al. (1986); [25] Palmer et al. (1989); [26] Chermak, Rimstidt (1989); [27] Holland (1989)

**Table 7** Sources of the reaction reversal data used as input in Bayesian analysis

| Reversed equilibria | Sources |
|---|---|
| 1 Ky = 1 And | Bohlen et al. (1991), Newton (1966b), Richardson et al. (1969), Holdaway (1971) |
| 1 And = 1 Si | Holdaway (1971), Heninger, Bowman (both in Holdaway and Mukhopadhyay 1993), Weill (1966) |
| 1 Ky = 1 Si | Newton (1966a), Bohlen et al. (1991), Richardson et al. (1968) |
| 1 aQz = 1 bQz | Mirwald and Massonne (1980) |
| 1 Cs = 1 aQz | Bohlen and Boettcher (1982) |
| 1 Cs = 1 bQz | Mirwald and Massonne (1980) |
| 1 And = 1 Co + 1 aQz | Harlov and Newton (1990) |
| 1 Ky = 1 Co + 1 bQz | Harlov and Newton (1993) |
| 1 Stv = 1 Cs | Zhang et al. (1996) |
| 1 Co + 1 Stv = 1 Ky | Schmidt et al. (1997) |
| 1 SWd + 1 Ky + 1 Cs = 2 Kfs | Urakawa et al. (1994), This study (Table 5c) |
| 1 Kls + 1 Kfs = 2 aLc | Scarfe et al. (1966), This study (Table 5a) |
| 1 Kls + 1 Kfs = 2 bLc | Scarfe et al. (1966), Lindsley (1966), This study (Table 5b) |
| 1 aLc = 1 bLc | Lange et al. (1986) |
| 1 Kls + 2 Cs = 1 Kfs | This study (Table 5d) |

**Table 8** Refined thermodynamic data for phases of the $K_2O$-$Al_2O_3$-$SiO_2$ system compared to the calorimetric input data used in Bayesian work. The *numbers in parentheses* are 2 standard deviations for the preceding quantity. *Asterisks* identify the reference phases

| Phase | Composition | Abbreviation | $H^\circ_{f,T^\circ}$ [J/mol] (input) | $H^\circ_{f,T^\circ}$ [J/mol] (refined) | $S^\circ_{T^\circ}$ [J/K · mol] (input) | $S^\circ_{T^\circ}$ [J/K · mol] (refined) |
|---|---|---|---|---|---|---|
| Andalusite | $Al_2[O\|SiO_4]$ | And | −2589900(2000) | −2589873(493) | 91.40(0.50) | 91.508(0.417) |
| Corundum* | $Al_2O_3$ | Co | −1675700(1300) | −1675700(0) | 50.92(0.10) | 50.917(0.100) |
| Coesite | $SiO_2$ | Cs | −907300(1200) | −907033(173) | 40.70(1.00) | 40.727(0.192) |
| K-feldspar* | $K[AlSi_3O_8]$ | Kfs | −3974600(3900) | −3974600(0) | 214.20(0.40) | 214.273(0.388) |
| Kalsilite | $K[AlSiO_4]$ | Kls | – | −2123846(2401) | 133.30(1.20) | 133.615(1.146) |
| Kyanite | $Al_2[O\|SiO_4]$ | Ky | −2593800(2000) | −2593856(458) | 82.80(0.50) | 82.790(0.367) |
| "Si-wadeite" | $K_2Si[Si_3O_9]$ | SWd | −4301150(5730) | −4301136(5646) | – | 232.107(10.447) |
| Sillimanite | $Al_2[O\|SiO_4]$ | Si | −2586100(2000) | −2586287(454) | 95.40(0.50) | 95.372(0.384) |
| Stishovite | $SiO_2$ | Stv | −873700(1600) | −872121(1224) | 27.30(1.00) | 26.202(0.698) |
| α-Leucite | $K[AlSi_2O_6]$ | aLc | – | −3029582(1266) | 200.20(1.70) | 198.438(1.104) |
| α-Quartz* | $SiO_2$ | aQz | −910700(1000) | −910700(0) | 41.46(0.20) | 41.467(0.109) |
| β-Leucite | $K[AlSi_2O_6]$ | bLc | – | −3023444(1498) | – | 205.486(1.036) |
| β-Quartz | $SiO_2$ | bQz | – | −908595(83) | – | 44.251(0.145) |

quantities with known expectation values and variances, by contrast, the estimated quantities are treated as uniformly distributed. As stated earlier, of all the quantities in Table 6, only $H^\circ_{f,T^\circ}$ and $S^\circ_{T^\circ}$ will be refined subject to the phase equilibria restrictions, excepting the reference $H^\circ_{f,T^\circ}$ of one phase per system component. The reference phases will be Kfs, Co and aQz; their $H^\circ_{f,T^\circ}$ will emerge unmodified in the refined thermodynamic dataset. Not included in Table 6 are the parameters from which the $G_{tr}$-term of Eq. (2) has been calculated. For phase transitions in quartz, leucite and kalsilite, the relevant parameters are given by Berman and Brown (1986) and Berman (1988). Carpenter and Salje's (1994) Landau formalism, which takes care of the microcline-sanidine transition as well as the non-convergent Al,Si order-disorder in sanidine, has been used to compute $G_{tr}$ in Kfs.

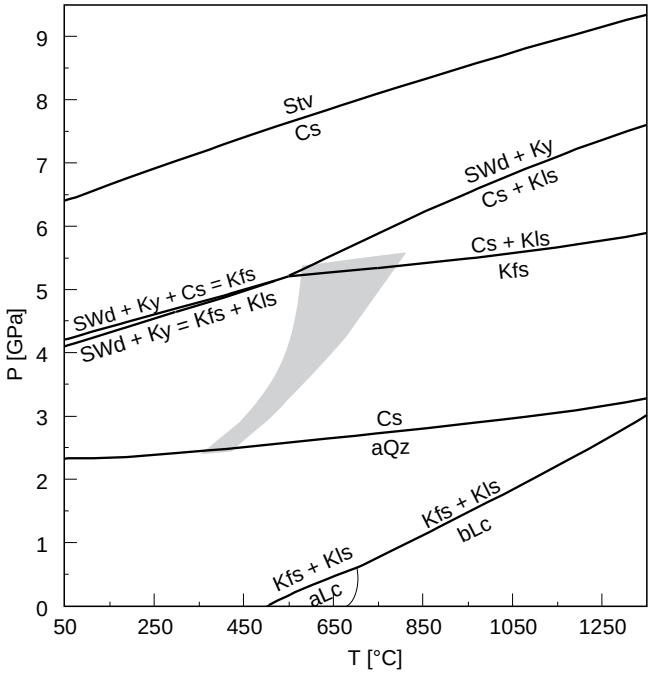


**Fig. 2** *P-T* diagram based on our refined thermodynamic dataset for the $K_2O$-$Al_2O_3$-$SiO_2$ ternary showing the pressure-induced decomposition of leucite and K-feldspar and the stability fields of α-quartz, coesite, and stishovite. The *stippled area* depicts the range of steady-state *P-T* paths followed by the top of a subducting oceanic crust for convergence rates between 1 and 10 cm/year (from Peacock et al. 1994)

## Reaction reversal data

Table 7 summarizes the sources of the reaction reversal data culled from the literature. They have been supplemented by our data given above. In all, 15 reactions are considered. In each case, the nominal *P*,*T* reversals have been expanded "away from the equilibrium" using the uncertainty of *P* and *T* indicated by the authors.

## Results

Table 8 documents the refined values for $H^\circ_{f,T^\circ}$ and $S^\circ_{T^\circ}$ of all phases and their $2\sigma$ uncertainties; not reproduced, for the sake of brevity, is the correlation matrix. The final values of $H^\circ_{f,T^\circ}$ and $S^\circ_{T^\circ}$, summarized in Table 8, were obtained by the Markov chain Monte Carlo technique called Gibbs sampling (cf. Olbricht et al. 1994).

We wish to focus on several aspects of the refined values of $H^\circ_{f,T^\circ}$ and $S^\circ_{T^\circ}$. First, they overlap with the corresponding input data within 1–$2\sigma$ range. Second, their $2\sigma$-uncertainties are now much smaller. Third, the $H^\circ_{f,T^\circ}$ of the reference phases (flagged by asterisks in Table 8) have not changed. And finally, the $H^\circ_{f,T^\circ}$ of Si-wadeite is in agreement with its revised value (see thermodynamic cycle reproduced in the Appendix), but its $S^\circ_{T^\circ}$ is larger than that computed by Geisinger et al. (1987) from their spectroscopic data. The larger $S^\circ_{T^\circ}$ is compatible with the systematically higher Cp observed by DSC in the subambient range (Fig. 1) compared to that derived from vibrational spectroscopy. We submit, however, that a calorimetric determination of $S^\circ_{T^\circ}$ of Si-wadeite will be necessary to verify our value. For now, we may conclude that the DSC data on the Cp(*T*) of

SWd has helped reconcile phase equilibria in the $K_2O$-$Al_2O_3$-$SiO_2$ ternary with the revised value of $H^\circ_{f,T^\circ}$ of Si-wadeite.

## Calculated phase relations and discussions

Using the refined values of $H^\circ_{f,T^\circ}$ and $S^\circ_{T^\circ}$ (Table 8) and the ancillary phase property data (from sources in Table 6), a *P-T* diagram for the system $K_2O$-$Al_2O_3$-$SiO_2$ can be generated. Figure 2 depicts, for clarity, just a few *P-T* curves to highlight the pressure-induced disproportionation of K-feldspar and leucite.

The decomposition of K-feldspar to the assemblage SWd + Ky + Cs becomes metastable at about 550 °C. Above that temperature, K-feldspar disproportionates to Cs + Kls at somewhat lower pressure than the metastable extension of the SWd + Ky + Cs = Kfs curve. A range of *P-T* trajectories for subduction regimes (Peacock et al. 1994), shown by stippling in Fig. 2, serves to emphasize that only the decomposition of Kfs to Cs + Kls is of relevance to nature. That notwithstanding, it is quite unlikely that pressure-induced decomposition of Kfs to Cs + Kls will be observed directly in rocks owing to the extremely high pressure required for that process, although coesite (Chopin 1984) and diamond (Sobolev and Shatsky 1990; Shutong et al. 1992) are known from rocks from subduction regimes. By contrast, leucite decomposes to Kls + Kfs at far lower pressures and has been reported from nature (Deer et al. 1992, p. 484).

**Acknowledgments** We are indebted to the Deutsche Forschungsgemeinschaft for funding a part of this research. Prof. A. Navrotsky kindly made available to us the revised value for the enthalpy of formation of Si-wadeite. We also thank Drs. P. Comodi and M.W. Schmidt, who shared with us their data on the compressibility and pressure-induced decomposition of kyanite prior to publication. Aid and advice given by Drs. P. Zinn, T. Peun, and K.-D. Grevel during the work at DESY are gratefully acknowledged. We thank Dr. H.-J. Bernhardt for the microprobe analysis. Constructive reviews of the draft of this paper by Drs. H. Behrens and J. Roux helped improve the presentation; we express our sincere appreciation for their effort.

**Appendix:** thermodynamic cycle for the enthalpy of formation of $K_2{}^{[VI]}Si[Si_3O_9]$ (SWd) from the stable elements at 298.15 K and 1 bar

| Reactions | $\Delta H(\pm 2\sigma)$ | Sources, remarks |
|---|---|---|
| $K_2Si_4O_9$(SWd 298 K) = $K_2Si_4O_9$ (SWd glass 973 K) | 279.66 (2.98) | Geisinger et al. 1987 |
| $K_2Si_4O_9$(SWd glass 973 K) = $K_2Si_4O_9$ (solution 973 K) | −21.79 (0.96) | Geisinger et al. 1987 |
| $K_2O$(crystal 298 K) = $K_2O$ (solution 973 K) | −193.68 (1.10) | Kiseleva et al. 1996 |
| $4{\cdot}SiO_2$(aQz 298 K) = $4{\cdot}SiO_2$(solution 973 K) | 4[39.10 (0.30)] | Kiseleva et al. 1996 |
| $K_2O$(crystal 298 K) + $4{\cdot}SiO_2$(aQz 298 K) = $K_2Si_4O_9$(SWd 298 K) | −295.15 (3.53) | Formation of SWd from the oxides |
| $2{\cdot}K + 0.5{\cdot}O_2 = K_2O$ (crystal 298 K) | −363.20 (2.10) | Robie and Hemingway (1995) |
| $4{\cdot}Si + 4{\cdot}O_2 = 4{\cdot}SiO_2$ (aQz 298 K) | 4[−910.7 (1.00)] | Robie and Hemingway (1995) |
| $2{\cdot}K + 4{\cdot}Si + 4.5{\cdot}O_2 = K_2Si_4O_9$ (SWd 298 K) | −4301.15 (5.73) | Formation of SWd from the elements |

## References


Akaogi M, Yusa H, Shiraishi K, Suzuki T (1995) Thermodynamic properties of α-quartz, coesite, and stishovite and equilibrium phase relations at high pressures and high temperatures. J Geophys Res 100(B11): 22337–22347

Angel RJ (1994) Feldspars at high pressure. In: Parsons I (ed) Feldspars and their reactions. NATO ASI Series C 421 pp 271–312

Appleman DE, Evans HT (1973) Job 9214: indexing and least squares refinement of powder diffraction data. US Dep Commerce Natl Tech Inf Serv PB 216 188

Berman RG (1988) Internally consistent thermodynamic data for minerals in the system $Na_2O$-$K_2O$-CaO-MgO-FeO-$Fe_2O_3$-$Al_2O_3$-$SiO_2$-$TiO_2$-$H_2O$-$CO_2$. J Petrol 29: 445–522

Berman RG, Brown TH (1985) Heat capacity of minerals in the system $Na_2O$-$K_2O$-CaO-MgO-FeO-$Fe_2O_3$-$Al_2O_3$-$SiO_2$-$TiO_2$-$H_2O$-$CO_2$: representation, estimation, and high temperature extrapolation. Contrib Mineral Petrol 89: 168–182

Berman RG, Brown TH (1986) Heat capacity of minerals in the system $Na_2O$-$K_2O$-CaO-MgO-FeO-$Fe_2O_3$-$Al_2O_3$-$SiO_2$-$TiO_2$-$H_2O$-$CO_2$: representation, estimation, and high temperature extrapolation (Erratum). Contrib Mineral Petrol 94: 262

Bohlen SR, Boettcher A (1982) The quartz ⇔ coesite transformation: a precise determination and the effects of other components. J Geophys Res 87: 7073–7078

Bohlen SR, Montana A, Kerrick DM (1991) Precise determination of the equilibria kyanite = sillimanite and kyanite = andalusite and a revised triple point for $Al_2SiO_5$ polymorphs. Am Mineral 76: 677–680

Brunet F, Vielzeuf D (1996) The farringtonite/$Mg_3(PO_4)_2$-II transformation: a new curve for pressure calibration in piston-cylinder apparatus. Eur J Mineral 8: 349–354

Carpenter MA, Salje EKH (1994) Thermodynamics of non-convergent cation ordering in minerals. III. Order parameter coupling in potassium feldspar. Am Mineral 79: 1084–1098

Chatterjee ND, Miller K, Olbricht W (1994) Bayes estimation: a novel approach to derivation of internally consistent thermodynamic data for minerals, their uncertainties and correlations. II. Application. Phys Chem Miner 21: 50–62

Chermak JA, Rimstidt JD (1989) Estimating the thermodynamic properties ($\Delta G^\circ_f$ and $\Delta H^\circ_f$) of silicate minerals at 298 K from the sum of polyhedral contributions. Am Mineral 74: 1023–1031

Chopin C (1984) Coesite and pure pyrope in high-grade blueschists of the western Alps: a first record and some consequences. Contrib Mineral Petrol 86: 107–118

Comodi P, Zanazzi PF, Poli S, Schmidt MW (1997) High-pressure behavior of kyanite: compressibility and structural deformations. Am Mineral 82: 452–459

Cox JD, Wagman DD, Medvedev VA (1989) CODATA key values for thermodynamics. Hemisphere Publishing Corp, New York

Decker DL (1966) Equation of state of sodium chloride. J Appl Phys 37: 5012–5014

Deer WA, Howie RA, Zussman J (1992) An introduction to the rock-forming minerals, 2nd edn. Longman, Harlow, UK

Endo S, Akai T, Akahama Y, Wakatsuki M, Nakamura T, Tomii Y, Koto K, Ito Y, Tokonami M (1986) High-temperature X-ray

study of single-crystal stishovite synthesized with $Li_2WO_4$ as flux. Phys Chem Miner 13: 146–151
Fasshauer DW, Chatterjee ND, Marler B (1997) Synthesis, structure, thermodynamic properties and stability relations of K-cymrite, $K[AlSi_3O_8] \cdot H_2O$. Phys Chem Miner 24: 455–462
Geisinger KL, Ross NL, McMillan P, Navrotsky A (1987) $K_2Si_4O_9$: energetic and vibrational spectra of glass, sheet silicate, and wadeite-type phases. Am Mineral 72: 984–994
Goranson RW, Kracek FC (1932) An experimental investigation of the phase relations of $K_2Si_4O_9$ under pressure. J Phys Chem 36: 913–926
Hamilton DL, Henderson CMB (1968) The preparation of silicate compositions by a gelling method. Mineral Mag 36: 832–838
Harlov DE, Newton RC (1993) Reversal of the metastable kyanite + corundum + quartz and andalusite + corundum + quartz equilibria and the enthalpy of formation of kyanite and andalusite. Am Mineral 78: 594–600
Hemingway BS, Robie RA, Evans HT, Kerrick DM (1991) Heat capacities and entropies of sillimanite, fibrolite, andalusite, kyanite, and quartz and the $Al_2SiO_5$ phase diagram. Am Mineral 76: 1597–1613
Hemley RJ, Prewitt CT, Kingma KJ (1994) High-pressure behavior of silica. In: Heaney PJ, Prewitt CT, Gibbs GV (eds) Silica (Reviews in mineralogy, 29) Mineral Soc Am, Washington, DC, pp 41–81
Henderson CMB, Taylor D (1988) The structural behaviour of the nepheline family. 3. Thermal expansion of kalsilite. Mineral Mag 52: 708–711
Höhne GWH, Cammenga HK, Eysel W, Gmelin E, Hemminger W (1990) The temperature calibration of scanning calorimeters. Thermochim Acta 160: 1–12
Holdaway MJ (1971) Stability of andalusite and the aluminum silicate phase diagram. Am J Sci 271: 97–131
Holdaway MJ, Mukhopadhyay B (1993) A reevaluation of the stability relations of andalusite: thermochemical data and phase diagram for the aluminum silicates. Am Mineral 78: 298–315
Holland TJB (1989) Dependence of entropy on volume for silicate and oxide minerals: a review and predictive model. Am Mineral 74: 5–13
Ito H, Kawada K, Akimoto S (1974) Thermal expansion of stishovite. Phys Earth Planet Inter 8: 277–281
Kelley KK, Todd SS, Orr RL, King EG, Bonnickson KR (1953) Thermodynamic properties of sodium-aluminum and potassium-aluminum silicates. US Bur Mines Rep Invest 4955: 1–21
Kinomura N, Kume S, Koizumi M (1975) Synthesis of $K_2SiSi_3O_9$ with silicon in 4- and 6-coordination. Mineral Mag 40: 401–404
Kiseleva I, Navrotsky A, Belitsky IA, Fursenko BA (1996) Thermochemistry of natural potassium sodium calcium leonhardite and its cation-exchanged forms. Am Mineral 81: 668–675
Komada N, Westrum EF, Hemingway BS, Anovitz LM (1995) Thermodynamic properties of two iron silicates: heat capacities of deerite from the temperature 10 to 700 K and of grunerite from 10 to 1000 K. J Chem Thermodyn 27: 1097–1118
Kroll H, Ribbe PH (1983) Lattice parameters, composition and Al,Si order in alkali feldspars. In: Ribbe PH (ed) Feldspar Mineralogy (Reviews in mineralogy, 2, 2nd edn) Mineral Soc Am, Washington, DC, pp 57–99
Kroll H, Schmiemann I, von Cölln G (1986) Feldspar solid solutions. Am Mineral 71: 1–16
Lange RA, Carmichael ISE, Stebbins JF (1986) Phase transitions in leucite ($KAlSi_2O_6$), orthorhombic $KAlSiO_4$, and their iron analogues ($KFeSi_2O_6$, $KFeSiO_4$). Am Mineral 71: 937–945
Lindsley DH (1966) *P-T* projection for part of the system kalsilite-silica. Geophys Lab Annu Rep 65: 244–247
Mirwald P, Massonne HJ (1980) The low–high quartz and quartz–coesite transition to 40 kbar between 600 and 1600 °C and some reconnaissance data on the effect of $NaAlO_2$ component on the low quartz–coesite transition. J Geophys Res 85: 6983–6990
Newton RC (1966a) Kyanite–sillimanite equilibrium at 750 °C. Science 151: 1222–1225
Newton RC (1966b) Kyanite–andalusite equilibrium from 700 to 800 °C. Science 153: 170–172
Olbricht W, Chatterjee ND, Miller K (1994) Bayes estimation: a novel approach to derivation of internally consistent thermodynamic data for minerals, their uncertainties and correlations. I. Theory. Phys Chem Miner 21: 36–49
Palmer DC, Salje EKH, Schmahl WW (1989) Phase transitions in leucite: X-ray diffraction studies. Phys Chem Miner 16: 714–719
Pankratz LB (1968) High-temperature heat contents and entropies of dehydrated analcite, kaliophilite, and leucite. US Bur Mines Rep Invest 7073: 1–8
Peacock SM, Rushmer T, Thompson AB (1994) Partial melting of subducting oceanic crust. Earth Planet Sci Lett 121: 227–244
Ralph RL, Finger LW, Hazen RM, Ghose S (1984) Compressibility and crystal structure of andalusite at high pressure. Am Mineral 69: 513–519
Richardson SW, Bell PM, Gilbert MC (1968) Kyanite-sillimanite equilibrium between 700 and 1500 °C. Am J Sci 266: 513–541
Richardson SW, Gilbert MC, Bell PM (1969) Experimental determination of kyanite–andalusite and andalusite–sillimanite equilibria; the aluminum silicate triple point. Am J Sci 267: 259–272
Richet P, Xu J, Mao HK (1988) Quasi-hydrostatic compression of ruby to 500 kbar. Phys Chem Miner 16: 207–211
Robie RA, Hemingway BS (1995) Thermodynamic properties of minerals and related substances at 298.15 K and 1 bar ($10^5$ Pascals) pressure and at higher temperatures. US Geol Surv Bull 2131
Robie RA, Hemingway BS, Fisher JR (1978) Thermodynamic properties of minerals and related substances at 298.15 K and 1 bar ($10^5$ Pascals) pressure and at higher temperatures. US Geol Surv Bull 1452
Sarge SM, Gmelin E, Höhne GWH, Cammenga HK, Hemminger W, Eysel W (1994) The caloric calibration of scanning calorimeters. Thermochim Acta 247: 129–168
Scarfe CM, Luth WC, Tuttle OF (1966) An experimental study bearing on the absence of leucite in plutonic rocks. Am Mineral 51: 726–735
Schmidt MW, Poli S, Comodi P, Zanazzi PF (1997) The high-pressure behavior of kyanite: decomposition of kyanite into stishovite and corundum. Am Mineral 82: 460–466
Shutong X, Okay AI, Shouyuan J, Sengör AMC, Wen S, Yican L, Laili J (1992) Diamond from the Dabie Shan metamorphic rocks and its implication for tectonic settings. Science 256: 80–82
Sobolev NV, Shatsky VS (1990) Diamond inclusions in garnets from metamorphic rocks: a new environment for diamond formation. Nature 343: 742–746
Stebbins JF, Kanzaki M (1991) Local structure and chemical shifts for six-coordinated silicon in high-pressure mantle phases. Science 251: 294–298
Susaki J, Akaogi M, Akimoto S, Shimomura O (1985) Garnet-perovskite transformation in $CaGeO_3$: in-situ X-ray measurements using synchrotron radiation. Geophys Res Lett 12: 729–732
Swanson DK, Prewitt CT (1983) The crystal structure of $K_2Si^{VI}Si^{IV}{}_3O_9$. Am Mineral 68: 581–585
Swanson DK, Prewitt CT (1986) Anharmonic thermal motion in $K_2Si^{VI}Si^{IV}{}_3O_9$(abstract). Eos Am Geophys Union 67: 369
Urakawa S, Kondo T, Igawa N, Shimomura O, Ohno H (1994) Sychrotron radiation study on the high-pressure and high-temperature phase relations of $KAlSi_3O_8$. Phys Chem Miner 21: 387–391
Waterwiese T, Chatterjee ND, Dierdorf I, Göttlicher J, Kroll H (1995) Experimental and thermodynamic study of heterogeneous and homogeneous equilibria in the system $NaAlSiO_4$-$SiO_2$. Contrib Mineral Petrol 121: 61–73
Weill DF (1966) Stability relations in the $Al_2O_3$-$SiO_2$ system calculated from solubilities in the $Al_2O_3$-$SiO_2$-$Na_3AlF_6$ system. Geochim Cosmochim Acta 30: 223–237
Zhang J, Li B, Utsumi W, Liebermann RC (1996) In situ X-ray observations of the coesite–stishovite transition: reversed phase boundary and kinetics. Phys Chem Miner 23: 1–10